

Competition between ultraviolet and infrared nanosecond laser pulses during the optical breakdown of KH_2PO_4 crystals

S. Reyné · G. Duchateau · J. Y. Natoli ·
L. Lamaignère

Received: 11 May 2012/Revised: 16 July 2012/Published online: 7 October 2012
© Springer-Verlag Berlin Heidelberg 2012

Abstract This study addresses the initiation of laser-induced breakdown of dielectric materials in the nanosecond regime under multi-wavelength conditions. In particular, the competition between multi-photon absorption and electronic avalanche as ionization mechanisms in KDP crystal is studied. Since they are both dependent on the laser frequency and intensity of incident radiations, we carried out two experiments: in mono-wavelength configuration at 1,064 nm and in multi-wavelengths configuration applying the simultaneous mixing of 1,064 and 355 nm radiations with various fluence ratios. To interpret experimental data, a model based on heat transfer and which includes ionization processes has been developed for both configurations. The comparison between experiments and modeling results first indicates that avalanche can be responsible for optical breakdown at 1,064 nm. Then, the study underlines the existence of a coupling effect in the multi-wavelength configuration where multi-photon absorption and electronic avalanche both contribute to the breakdown. From a general point of view, the model accounts for the experimental trends and particularly reveals that the electronic recombination timescale may have an important role in the scenario of nanosecond laser-induced breakdown.

1 Introduction

With the development of high-power lasers, laser-induced breakdown phenomenon in dielectric materials has given rise to many interrogations on its origins. The numerous studies carried out for various condensed media [1–4], laser frequencies [5, 6] or pulse durations [7–11] highlight the complexity of the physical processes involved. Briefly, the absorption of a laser radiation leads to the ionization of the material which results in the formation of a plasma. The latter can absorb the radiation and induce a large increase in temperature that may lead to breakdown. The generation of free electrons in large amount may be due to non-linear processes such as multi-photon ionization (referred to as MPI) or impact ionization (referred to as II). Their efficiencies are strongly dependent on the wavelength, the duration and the intensity of the laser pulse. From a modeling point of view, the roles of MPI and II in optical breakdown have been either considered separately [1, 12, 13] or in wavelength mixing cases [8, 14, 15]. Short wavelengths mainly induce MPI, while longer ones induce II. Beyond these considerations, classical theories developed to study pure wide-bandgap dielectrics fail or sometimes lead to controversial assessments [5, 7, 16]. Some conclusions generally concur with the existence of a competition between these two mechanisms [14]. Others highlight their cooperation: MPI can initiate II by providing seed electrons which are required for engaging electronic avalanche. Particularly, the existence of this coupling effect has been observed recently in potassium dihydrogen phosphate crystals (KH_2PO_4 or KDP) [17, 18].

KDP is a wide-bandgap dielectric material which has been studied for decades due to its good electro-optical properties. In particular, it is used as frequency converters in the context of laser facilities such as the National

S. Reyné (✉) · L. Lamaignère
CEA-Cesta, 15 Avenue des Sablières, 33114 Le Barp, France
e-mail: stephane.reyne@free.fr

S. Reyné · G. Duchateau
CELIA, UMR-5107 Université Bordeaux I-CNRS-CEA,
351 Cours de la libération, 33405 Talence, France

J. Y. Natoli
Institut Fresnel, UMR-CNRS 6133, D.U. St Jérôme,
13397 Marseille, France

Ignition Facility in the USA and the Laser MegaJoule in France. For these megajoule-class lasers, KDP components are exposed during a few nanoseconds (ns) to pulses with wavelengths ranging from infrared (1,053 nm or 1ω) to ultraviolet (351 nm or 3ω). Also, energy densities possibly reach few tens of J/cm², which are large enough to induce laser damage in the bulk of these crystals (see for instance [6, 19] and references therein). In the nanosecond regime, Carr et al. [6] have shown MPI to be responsible for damage in KDP for $\lambda < 532$ nm. It appears that multi-photon absorption is assisted by defect-induced states located in the bandgap. These states are induced by precursor defects whose size most probably ranges from ten to hundreds of nanometers [20].

In the present study, we propose an original approach based on the wavelength dependence of MPI and II mechanisms to discriminate their role in the optical breakdown of KDP crystals in the ns regime. This approach relies on the comparison between experimental and modeling results. First, the experimental part consists in a pump–pump test implying the simultaneous exposure of a KDP crystal to radiations with different wavelengths: 3ω and 1ω . In this configuration, we observe the breakdown occurrences for various fluences combinations of each pulses. The modeling part relies on a semi-analytic approach describing the ns heating of nanometric precursor defects at 3ω , hereafter referred to as DMT _{3ω} model [21]. This model has already succeeded to explain most of the experimental trends observed for the ns laser damage of KDP at 3ω [6, 18, 21, 22, 23, 24, 25]. The DMT _{3ω} model is based on the fact that conduction band electrons are produced at the beginning of the pulse (about 10²² electrons/cm³ at 3ω) and then heated during the whole pulse duration [20, 21]. To be representative of the multi-wavelength experimental configuration, DMT _{3ω} has been adapted to the situation where 1ω and 3ω radiations are simultaneously present. This results in the DMT _{2λ} model which

differs from DMT _{3ω} , particularly due to its adaptation at 1ω , by including II. This approach justifies *a posteriori* the contribution of each wavelength to electronic plasma production and heating. Next, a comparison between the experimental data and the DMT _{2λ} model is proposed. In the present conditions, this approach allows one to identify the physical processes of energy coupling involved. Furthermore, it permits evaluating the value of parameters driving the laser–matter interaction, as for instance multi-photon absorption cross sections or recombination time. The latter value is confirmed by a specific experiment including time delay between both pulses.

2 Experimental setup

2.1 Facility

The experimental study was performed in the laser damage facility BLANCO (Banc Laser Nanoseconde pour Composants Optiques, see Fig. 1) at CEA/CESTA in France [26]. This facility is based on a Q-switched Nd:YAG laser giving access to 1ω and 3ω radiations. Each wavelength is separated in a different pathway, which permits performing damage tests with either a single or two wavelengths simultaneously. The 1ω and 3ω equivalent pulse durations (defined as the ratio of the total energy to peak power) are 6.5 and 5.5 ns, respectively. A 100 mW–CW laser diode seeder ensures the temporal profile to be mono-mode longitudinal and stable. At the exit, the laser delivers approximately 800 mJ (at 1ω) and 130 mJ (at 3ω) at a nominal repetition rate of 10 Hz. Energy on the sample is adjusted through a system “ $\lambda/2$ -plate-polarizer”. For each wavelength, the laser beam is P-polarized and its polarization remains unchanged during the tests. Each laser beam is then focused on to the sample by a convex lens whose focal length is approximately 4,000 mm. This induces a

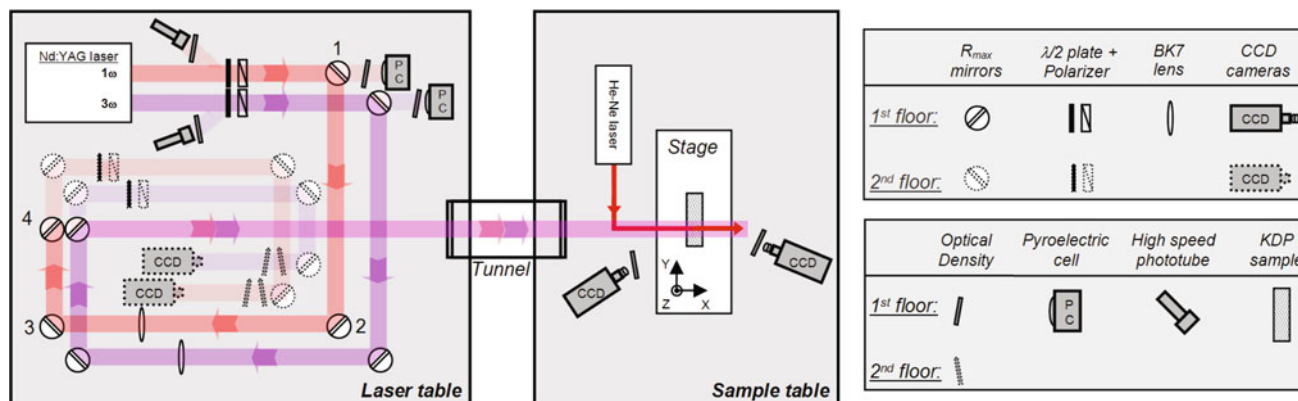


Fig. 1 The BLANCO laser damage facility. The Nd–YAG fundamental (1ω) and third harmonic (3ω) beams are used for the damage tests whose procedure is presented in Sect. 2.2. The diagnostics to monitor the laser beams characteristics are presented in Sect. 2.1 (see text)

depth of focus (DOF) higher than the sample thickness, ensuring the beam shape to be constant along the DOF. At the focus region, beam spots are millimetric, Gaussian-shaped and the diameters (given at $1/e$ for a Gaussian beam) are $700\text{ }\mu\text{m}$ at 1ω and $450\text{ }\mu\text{m}$ at 3ω . As a consequence, fluences available on this facility may reach about 150 and 70 J/cm^2 , respectively, at 1ω and 3ω .

2.2 Procedure

The tests were performed according to a one-on-one procedure [27]. During a test, the laser shots characteristics are measured: the energy E and the beam area giving access to the fluence F (in J/cm^2), and the temporal profile. The absolute fluence is determined with an accuracy of as much as $\pm 10\%$ [19]. The damage pinpoints appear in the bulk of the crystal and an in situ detection system is thus required. It consists in a volumic detection thanks to the scattering of a He–Ne laser beam propagating collinearly to the test beam. This procedure enables determining a damage probability P_{dam} as a function of the fluence F . Given the irradiated volume, results are plotted for volumic damage densities ρ_{dam} (in damages per mm^3 or dam./mm^3) obtained by converting the damage probability P_{dam} [28]. Due to the experimental procedure and beam size, the lower limit of damage detection is around 10^{-2} dam./mm^3 . For the tests carried out in the multi-wavelength case, it is necessary to measure each beam and each detector being duplicated on each pathway. The tests permit extracting the damage density as a function of the fluences couples ($F_{1\omega}, F_{3\omega}$). Also, the equivalent volume to define ρ_{dam} is determined by considering that the laser interaction volume corresponds to the region where the 3ω and 1ω beams overlap.

2.3 Samples

The KDP samples, referenced as KDP # A and KDP # B, used in experimental tests, originate from the prismatic sector of a rapidly grown boule. It consists of pristine plates whose dimensions are $100 \times 100 \times 10\text{ mm}^3$. Sample # A is cut for type-II third harmonic generation where damage tests had been performed in the mono-wavelength case with fluences at 1ω ranging from 14 to 24 J/cm^2 . For sample # A, the lower experimental limit of damage detection would appear in the mono-wavelength case for fluence at 1ω above 11 J/cm^2 . Sample # B is cut for type-I third harmonic generation where damage tests had been performed in the multi-wavelength case with fluences at 1ω and at 3ω covering the range of $[0\text{--}35]\text{ J/cm}^2$ and $[0\text{--}14]\text{ J/cm}^2$, respectively. For sample # B, the damage densities of 10^{-2} dam./mm^3 appear in the mono-wavelength cases for fluences around 7 and 18 J/cm^2 , at 3ω and 1ω ,

respectively. The study in the 1ω mono-wavelength case have been performed on KDP # A, while on KDP # B for the multi-wavelength case. It turns out that the discrepancies in the damage resistance between these two crystals is not a critical point.

3 Study in the mono-wavelength case: 1ω

The model proposed here is based on the DMT model (for Drude–Mie–Thermal model, see Appendix 1) developed by Dyan et al. [21] at 3ω . This model considers that a nanometric precursor defect transforms into a plasma instantaneously through defect-assisted MPI. Basically, this model solves the Fourier's equation on a timescale corresponding to the whole pulse duration and provides a direct link between the laser fluence and the temperature elevation of the plasma. Nevertheless, trying to generalize this model at 1ω would lead to misinterpretations, since the hypothesis of instantaneous plasma formation fails as shown hereafter.

3.1 Avalanche model: description

From a phenomenological point of view at 1ω , the probability of electrons to transit from the valence band (VB) to the conduction band (CB) due to MPI is considerably reduced, since seven photons at 1.18 eV are required to bridge the 7.8 eV KDP bandgap [29]. An alternative to produce electrons is impact ionization, which is efficient at long wavelengths [5, 15, 16]. Hereafter, an analysis is proposed to state whether this mechanism may occur within our conditions. Stuart et al. [16] have defined a criterion providing the intensity for which avalanche becomes the dominant ionization mechanism. It corresponds to an intensity level $I_{\text{cr}} (\propto E^2)$ defined by $\sigma(0)E^2 > U_{\text{ph}}\gamma(0)$, where $\sigma(0)$ corresponds to the electronic conductivity (which can be evaluated by a Drude model [30]), E is the electric field of radiation, U_{ph} is the optical phonon energy and $\gamma(0)$ is the rate of transfer of energy from electrons to the crystal lattice. A crude evaluation of I_{cr} indicates that several tens of GW/cm^2 may be enough for avalanche to engage at 1ω . Given the experimental conditions used in this study, these fluences are consistent with the existence of an avalanche mechanism. Schematically, the evolution of electrons in the CB can be represented by Fig. 2 within this scenario.

Figure 2 shows the three different stages: (1) a moderate production of electrons during t_{prod} probably due to MPI where n_e remains low compared to the critical plasma density n_c , (2) an exponential growth due to the fast multiplication of electrons by II and (3) their heating possibly leading to damage. Since it is now assumed at 1ω that the

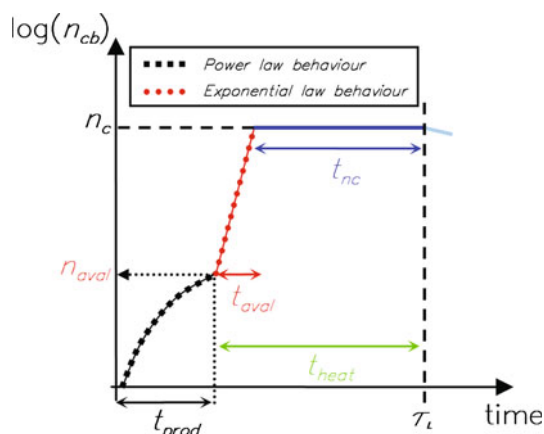


Fig. 2 Schematic of the temporal evolution of the electronic density n_{cb} in the CB at 1ω . Three stages are suggested, associated with various times: t_{prod} , t_{aval} and t_{heat} (see text below). These times successively correspond to the production time of prime electrons, the avalanche time and the heating time of the plasma ball

absorbing plasma ball is no more produced at the very beginning of the pulse, we introduce a heating time called t_{heat} (see Fig. 2) which corresponds to the duration of a significant plasma ball heating, i.e., when n_{cb} is close to n_c . As shown on Fig. 2, there is an implicit relation between t_{prod} and t_{heat} , which is governed by the starting of the avalanche.

To define a criterion for avalanche to engage, we generalize the work of Noack and Vogel [31] which describes the evolution of the electronic density and plasma property in water for various pulse durations. To engage the avalanche mechanism, they assumed that at least one electron was present in the irradiated volume. We propose here to adapt their concept to the case of defects present in KDP. This approach is realistic, since water can be considered as a large bandgap dielectric. So it is assumed that provided at least one CB electron is produced in the volume of a defect, the mechanism of successive impact ionizations can initiate an avalanche in the defect. This condition, proposed in our model as the avalanche criterion, corresponds to the electronic density n_{aval} reached in the volume of a defect whose radius a , is defined by:

$$n_{aval} = n_0 \times \left(\frac{a_0}{a}\right)^3 [\text{cm}^{-3}] \quad (1)$$

where n_0 corresponds to an electron density obtained in a defect with a radius of reference a_0 . As it exists in the DMT model as a direct link between the precursors and the damage densities [see Appendix 1, Eq. (10)], it follows that n_{aval} must be dependent on the precursor size a and compatible with the size distribution to be representative of the experimental damage densities. It then results that $n_0 \simeq 10^{14} \text{ cm}^{-3}$ and $a_0 = 100 \text{ nm}$. The latter value is also confirmed as a good indicator of precursor size, since its value is close to the thermal diffusion length $L_{th} = \sqrt{4\kappa_{KDP}\tau_L}$ where κ_{KDP} is the

KDP thermal diffusivity and τ_L is the pulse duration. Thus, assuming that optical breakdown at 1ω is mainly due to II, it is necessary to reach the avalanche criterion in a time t_{prod} shorter than the pulse duration.

As usual, the electronic density evolution can be described by a rate equation [4, 11], which has been simplified in this study as follows:

$$\frac{\partial n_{cb}}{\partial t} = W_{MPI} - \frac{n_{cb}}{\tau_r} \quad \text{for } t < t_{prod} \quad (2)$$

where $W_{MPI} = n_{vb}\sigma_m\Phi_{ph}^m$ is the multi-photon ionization rate, n_{vb} the valence-band electrons density, σ_m the m -photon absorption cross section, Φ_{ph} the photon flux, and m the number of photons implicated in the multi-photon process. Note that σ_m can be significantly enhanced by defect-induced states. It reflects the influence of the precursor defects which can assist and enhance the absorption process (see also the discussion in Sect. 4.3). τ_r corresponds to the recombination time. This model considers that at $t = 0$, $n_{cb} = 0$. As the electronic density evolves with an exponential growth due to the cascade ionization mechanism, we may reasonably consider that $t_{aval} \ll \tau_L$. It is thus assumed that when $t > t_{prod}$, n_{cb} saturates to n_c , where $n_c \simeq 9.8 \times 10^{20} \text{ cm}^{-3}$ at 1ω . An analytical expression of t_{heat} can be then derived from Eq. (2) (see Appendix 2.1):

$$t_{heat} = \tau_L + \tau_r \times \ln\left(1 - \frac{n_{aval}}{n_{vb}\sigma_m\Phi_{ph}^m\tau_r}\right). \quad (3)$$

According to Eq. (3), there is a direct link between the electron production (which depends on the radiation fluence at 1ω) and the time t_{heat} of plasma heating. So under this new framework, referred to as DMT $_{1\omega}$, heat transfer can be addressed by solving the Fourier's equation on the timescale $t = t_{heat}$. Finally, by introducing a defect distribution [20, 26], it is possible to extract the evolution of the damage density ρ_{dam} as a function of the fluence at 1ω (see Appendix 1).

Note that some other contributions such as non-radiative relaxations may also participate in the temperature rise of the lattice [25], but are not included in the present work. The plasma ball is defined by its complex optical indices and size necessary to solve the Fourier's equation (see Appendix 1). As $n_{cb} = n_c$ for $t > t_{prod}$, we consider that $n_{1\omega}$ and $k_{1\omega}$ are constant. Also, considering defects whose size range is similar to the one of 3ω defects is consistent with experimental observations. Indeed, it has been observed experimentally that in the ns regime 1ω and 3ω laser damage can be obtained in KDP with damage fluences which lie in the same range. Furthermore, we also consider that the volume of the defect does not evolve with time (i.e., no hydrodynamics).

3.2 Results and discussion

Figure 3 presents the experimental and modeling results obtained in the 1ω mono-wavelength case for sample # A. Experimental data (triangles) are compared to the modeling results (in dashed and dotted lines) obtained with the DMT model. To evaluate the reliability of DMT $_{1\omega}$ (in dotted lines), a comparison with DMT $_{3\omega}$ (in dashed lines) is proposed.

Experimental results can be fitted with a power law (in solid line) such as $\rho_{\text{dam}} = \alpha \cdot F_{1\omega}^\beta$ (see Appendix 1), where α and β are free parameters. For this test, we find that $\alpha = 2.45 \times 10^{-8}$ and $\beta = 5.2$. The DMT $_{1\omega}$ model provides predictions in a better agreement with experimental results than the DMT $_{3\omega}$ model. Indeed, at the lowest and highest damage densities, the predictions diverge more rapidly from the power law than with the DMT $_{1\omega}$ model. The parameters used in the model DMT $_{1\omega}$ are reported in Table 1. This set of parameters is adjusted to obtain the best agreement with experimental results. For the following parts of the study, the obtained values have been kept constant. Note that the slight variations of these parameters provide the same trends and do not modify our conclusions.

Based on the fact that the model is in agreement with experimental results, it confirms that avalanche can be responsible for laser-induced breakdown at 1ω . While considering MPI and II separately as mechanisms that can lead to breakdown, these mechanisms may compete when wavelengths are mixed, particularly due to their wavelength sensitivity. This configuration is addressed in the

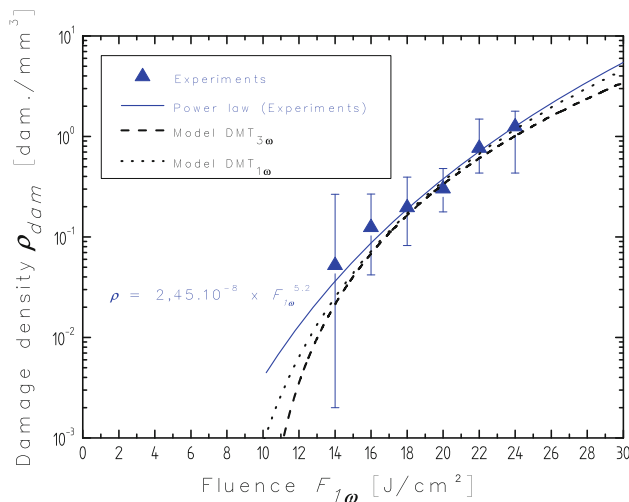


Fig. 3 Evolution of the laser-induced damage density ρ_{dam} as a function of the fluence $F_{1\omega}$. Experimental results (triangles) follow a power law [see Appendix 1, Eq. (13)]. Experiments are compared with modeling curves obtained with the DMT model in the “ 3ω ” framework (DMT $_{3\omega}$, in dashed lines) where the Fourier’s equation resolution is done on $t_{\text{heat}} = \tau_L$ and the “ 1ω ” framework (DMT $_{1\omega}$, in dotted lines) where the Fourier’s equation resolution is done on $t_{\text{heat}} = f(F_{1\omega})$ (see text)

Table 1 Parameters used in the DMT $_{1\omega}$ model (i.e., the mono-wavelength case) for the pulse at 1ω

Parameters	Value	Definition
λ	1,064 nm	Wavelength of the laser pulse at 1ω
τ_L	6.5 ns	Pulse duration at 1ω
T_c	6,000 K	Critical temperature to induce a damage
$(n_{1\omega}, k_{1\omega})$	(0.30, 0.11)	Optical indices (real and imaginary part) at 1ω during t_{heat}
a	[10–200] nm	Size range of the precursor defects
m	See Sect. 4.3	Number of photons implied in the multi-photon process
σ_m	Depends on the value of m	m -photon absorption cross section
τ_r	Few hundreds of ps	Recombination time of conduction electrons
(C, p)	$(2.5 \times 10^{-47}, 7.5)$	Parameters defining the size distribution of defects

next section where we present a model, referred to as the DMT $_{2\lambda}$, which takes into account avalanche and multi-photon ionization as processes possibly responsible for laser damage.

4 Study in the multi-wavelength case: 1ω and 3ω

4.1 Model DMT $_{2\lambda}$

To address the multi-wavelength case, we suggest a model based on the previous experimental and modeling work carried out for these two wavelengths [18] under conditions where $F_{3\omega} > F_{1\omega}$. This model has shown indeed that a 3ω -multi-photon mechanism is responsible for the fast production of conduction electrons. A limitation concerns the contribution of an avalanche mechanism which had not been taken into account due to the low 1ω fluences involved during experiments. Given the intensity levels used at 1ω in the present study, it is relevant now to introduce in DMT $_{2\lambda}$ the avalanche model presented in Sect. 3. We then consider in this model that MPI and II can be mechanisms responsible for breakdown which now permit extending its domain of validity on a wide range of fluences at 1ω and 3ω . Along the same modeling baseline developed in [18] and in Sect. 3, the DMT $_{2\lambda}$ model considers a size distribution of independent spherical defects whose temperature rise is driven by heat transfer. By introducing a defects distribution, the evolution of the damage density ρ_{dam} can be extracted and is consequently given as function of the fluences at 1ω and 3ω .

Similarly to the 1ω modeling framework, the DMT $_{2\lambda}$ model solves the Fourier’s equation on the so-called

heating time t_{heat} which now depends on the fluences at 1ω and 3ω , since we suppose that each wavelength participates in the production of CB electrons. The analytical derivation of t_{heat} in the multi-wavelengths case is quite similar to the one given in the mono-wavelength case by Eq. (3) (see Appendix 2.2 for more details). The DMT_{2λ} model considers a single size distribution where precursor defects are supposed to be both sensitive to 1ω and 3ω [18]. It then results that in the simultaneous presence of two wavelengths, a precursor defect absorbs the incident radiations as follows:

$$Q_{\text{abs}}^{(3\omega)}(3\omega, 1\omega)I_{3\omega} + Q_{\text{abs}}^{(1\omega)}(3\omega, 1\omega)I_{1\omega} \quad (4)$$

where $Q_{\text{abs}}^{(3\omega)}(3\omega, 1\omega)$ and $Q_{\text{abs}}^{(1\omega)}(3\omega, 1\omega)$ are the absorption efficiencies at 3ω and 1ω . Also, it has been shown that when $F_{3\omega}$ is larger than $F_{1\omega}$ [18]:

$$\begin{cases} Q_{\text{abs}}^{(3\omega)}(3\omega, 1\omega) = Q_{\text{abs}}^{(3\omega)}(3\omega) \\ Q_{\text{abs}}^{(1\omega)}(3\omega, 1\omega) = \beta F_{3\omega}^\delta + Q_{\text{abs}}^{(1\omega)} \end{cases} \quad (5)$$

Before comparing the DMT_{2λ} model with the multi-wavelength experimental results, we have checked that the model accounts for the limit cases (i.e., the 1ω and 3ω mono-wavelength cases):

- When $F_{3\omega} \rightarrow 0$, $t_{\text{heat}} = f(F_{1\omega})$, $Q_{\text{abs}}^{(1\omega)}(3\omega, 1\omega) \simeq Q_{\text{abs}}^{(1\omega)}$ and $Q_{\text{abs}}^{(3\omega)}(3\omega, 1\omega)I_{3\omega} \rightarrow 0$. This configuration becomes similar to the mono-wavelength case at 1ω .
- On the contrary, when $F_{1\omega} < F_{3\omega}$, $t_{\text{heat}} = \tau_L$. This configuration corresponds to the multi-wavelength configuration previously studied in [18].

4.2 Experimental and modeling results

Figure 4 represents the damage iso-densities obtained on sample # B, which exhibits a particular pattern: given a damage density, the lower the fluences $F_{3\omega}$, the higher are the fluences $F_{1\omega}$. We thus tried to make a connection between the fluences $F_{1\omega}$ and $F_{3\omega}$ and the ionization mechanisms responsible for breakdown. It has been previously shown in [18] that a combination of $(F_{3\omega}, F_{1\omega})$ can be equivalent in terms of damage density level to an equivalent fluence at 3ω . We then define $F_{3\omega}^{(\text{eq})}$ as the 3ω -equivalent fluence that induces the same damage density than the one obtained with any couple of fluences $(F_{3\omega}, F_{1\omega})$. This relation can be defined by the following equation:

$$F_{3\omega}^{(\text{eq})} = f(F_{3\omega}, F_{1\omega}) \simeq sF_{1\omega} + F_{3\omega} \quad (6)$$

where s is defined as the slope of an iso-density. It turns out that this quantity reveals the existence of a coupling effect between 1ω and 3ω . The parameter s thus contains the

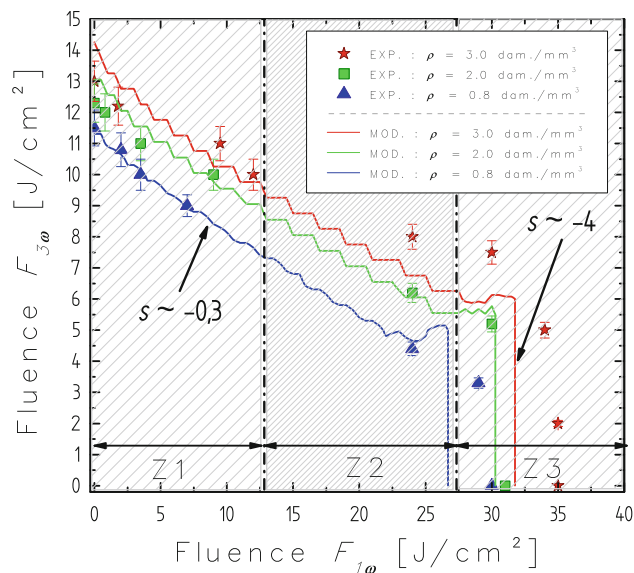


Fig. 4 Laser-induced damage density ρ_{dam} as a function of the fluences $F_{3\omega}$ and $F_{1\omega}$. Experimental results are represented by stars, triangles and squares. Modeling results (will be discussed in Sect. 4.3) are represented by solid lines. Parameter s indicates the slope of damage iso-densities

main physical information about the coupling process between these two wavelengths [18]. In the following, we then focus our attention on this parameter. A quick overview of Fig. 4 indicates that s is not constant on the whole range of fluences $F_{3\omega}$ and $F_{1\omega}$. Indeed, we suggest that this pattern can be separated into three zones referred to as Z1, Z2 and Z3. These three zones are defined considering that a variation of s is significantly different from a zone to another. Note that the values of s are obtained by a linear fit in each zone (not represented on Fig. 4) and read as follows:

- Z1: s gently slopes and its value is approximately -0.3 . It corresponds to the multi-wavelength configuration as observed in [18].
- Z2: s cannot be determined due to the lack of experimental data in this zone. We assume that s follows a steady decrease, but it is difficult to be more precise from an experimental point of view.
- Z3: s exhibits a sharp decrease which results in a value close to approximately -4 . It corresponds to the mono-wavelength limit case at 1ω .

In Z1, the value of s suggests that there is a coupling effect between the two radiations as previously explained [18]. Although we lack experimental data for Z2, we assume that Z2 may be considered as a “transition zone” between Z1 and Z3. In Z3, a radical change is observed and its value clearly indicates a change in the coupling mechanism where the damage densities are almost independent of the

fluences at 3ω . It seems to be an indication that 1ω may be dominant, due to the high levels of $F_{1\omega}$ compared to $F_{3\omega}$.

One can see on Fig. 4 that the modeling results are in good agreement with the experimental ones: in Z1 and Z3, the modeling slopes s are consistent with the experimental data. The model also predicts the trend in the zone Z2: it indicates a steady decrease, which seems appropriate if Z2 can be considered as a transition between Z1 and Z3. This confirms a posteriori that there is no change in the mechanisms between Z1 and Z2. Also, the DMT_{2λ} model points out the existence of dominant mechanisms in the limit cases: when $F_{3\omega}$ is large compared to $F_{1\omega}$, the multi-photon process dominates and avalanche is almost inefficient. On the contrary, the domination of avalanche occurs when fluences $F_{1\omega}$ become much larger than fluences $F_{3\omega}$.

4.3 Discussion

In the literature, few studies comparing both experiments and modeling in the ns regime report the influence of combined radiations on the laser-induced breakdown [8, 14, 15, 17, 18]. All of the experimental results or predictions in these former studies indicate a competition between these two mechanisms. Precisely due to a direct comparison with experimental results as seen on Fig. 4, the DMT_{2λ} model highlights the change in the value of the slope s for particular pairs of fluences ($F_{1\omega}, F_{3\omega}$). This can be associated with a change in the coupling between a 3ω multi-photon absorption process and an avalanche mechanism at 1ω . It results in the following:

- In zone Z3, when $F_{1\omega} \gg F_{3\omega}$, avalanche dominates compared to a multi-photon process.
- In zones Z1 and Z2, there is a cooperation between MPI and II when $F_{3\omega}$ and $F_{1\omega}$ are in a ratio close to one-third (1:3).

As the model is mainly of interest in the general trends obtained from Fig. 4, it is actually difficult to be more quantitative on the breakdown scenario.

Now, we propose an analysis to identify the parameters which play an important role and discriminate their influence on the modeling results plotted in Fig. 4. The set of parameters used in the DMT_{2λ} model is reported in Table 2 and has been adjusted to obtain the best agreement with experimental results. Note that these parameters have been tested independently. In the model, the absorption cross sections σ_3 and σ_7 have been fixed to fulfill the mono-wavelength cases. Once fixed, these parameters have remained constant during the whole modeling in the multi-wavelength case. It is worth noting that their values implicitly account for assisted transitions. It follows that their values do not correspond to the empiric ones determined by Agostini et al. [32]. However, we did not observe

Table 2 Parameters used in the DMT_{2λ} model (i.e., the multi-wavelength case) for the pulses at 1ω and 3ω

Parameters	Value	Definition
λ_1	1,064 nm	Wavelength of the laser pulse at 1ω
λ_3	355 nm	Wavelength of the laser pulse at 3ω
$\tau_L^{1\omega}$	6.5 ns	Pulse duration at 1ω
$\tau_L^{3\omega}$	5.5 ns	Pulse duration at 3ω
T_c	6,000 K	Critical temperature to observe a damage
$(n_{1\omega}, k_{1\omega})$	(0.30, 0.11)	Optical indices (real and imaginary part) at 1ω
$(n_{3\omega}, k_{3\omega})$	(0.30, 0.15)	Optical indices (real and imaginary part) at 3ω
a	[10–200] nm	Size range of the precursor defects
m	$3 \leq m \leq 7$, most probably 3	Number of photons implied in the multi-photon process
$\sigma_{m=3}$	$8.4 \times 10^{-94} \text{ m}^6 \text{ s}^{-2}$	3-photon absorption cross section
$\sigma_{m=7}$	$1.3 \times 10^{-226} \text{ m}^{14} \text{ s}^{-6}$	7-photon absorption cross section
τ_r	See Sect. 4.3	Recombination time
(C, p)	$(2.5 \times 10^{-47}, 7.5)$	Parameters defining the size distribution of defects

a strong influence on the slope s by changing the number of photons from three to seven at 1ω . It turns out that a consecutive absorption of seven photons is less probable due to the weak resulting absorption cross section compared to a three-photon absorption cross section. Nevertheless, n -photon absorption processes are not excluded, with $3 < n < 7$, indicating that non-radiative recombinations would occur. Indeed, electrons which do not acquire sufficient energy to bridge the bandgap may recombine and then participate in the lattice temperature elevation.

Concerning the density of defects N_{def} , previous studies [26, 33–36] have suggested that several populations sensitive to different wavelengths may exist in KDP. As it is difficult to prove the existence of different classes of precursors, we choose considering a single population of defects to simplify the interpretation of results. This population is then supposed to be both sensitive to 1ω and 3ω radiations. Also, the size distribution chosen in the model seems consistent with the experimental results. Indeed, the avalanche mechanism is all the more probable as the precursor defects are larger, because it is easier to promote at least an electron in the volume of the defect. It follows that the Z3 avalanche is more likely to occur for precursor defects of larger radii.

Concerning the heating time, t_{heat} is directly linked to the fluences $F_{1\omega}$ and $F_{3\omega}$. Fig. 5 represents its evolution as a function of $F_{1\omega}$ and $F_{3\omega}$. It appears that the evolution of the modeling trends are correlated to the ones of t_{heat} . Long

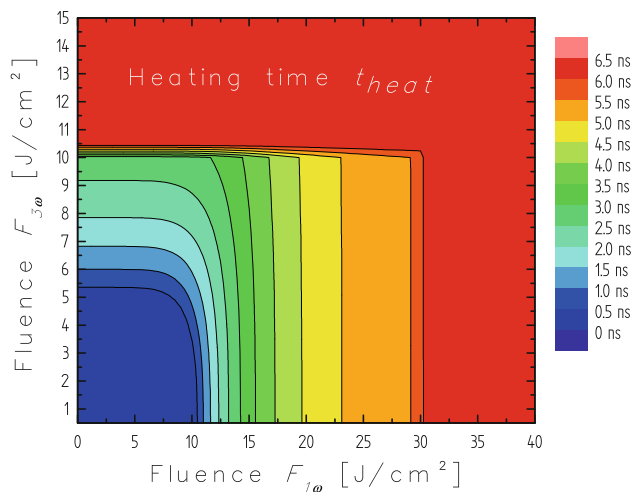


Fig. 5 Evolution of t_{heat} as a function of the fluences $F_{1\omega}$ and $F_{3\omega}$. This graph indicates the implication of MPI and II in the coupling as a function of the fluences $F_{3\omega}$ and $F_{1\omega}$

times are the result of fast generation of free electrons and may then contribute to an efficient plasma heating (the 1ω radiation being more efficient than the 3ω for plasma heating). On the contrary, short times indicate that both production and heating would not operate at a sufficient rate to induce breakdown.

As a consequence, the parameters influencing the DMT_{2λ} model are synthesized and reported in Table 3. It turns out that the most influent parameter is the recombination time τ_r . First, we have observed that a constant value for τ_r is not appropriate to account for the experimental results. Then, we propose different evolutions of τ_r as function of $(F_{3\omega}, F_{1\omega})$ and the modeling results associated to each case. We conclude that for the limit cases (i.e., only $F_{3\omega}$ or only $F_{1\omega}$), longer recombination times (about 1,500 ps) are suitable to mimic trends defined by $s \simeq -0.3$. On the contrary, smaller times (close to 100 ps)

Table 3 DMT_{2λ} model parameters and their influence on multi-wavelength results

Parameters used in the DMT _{2λ} model	Influence on the following parameters		
	Levels of fluences	Levels of damage densities	Slopes
Critical temperature T_c	✓		
Absorption cross sections σ_3, σ_7	✓		
Heating time t_{heat}			✓
Absorption efficiencies \mathcal{Q}_{abs}			✓
Precursor defects distribution N_{def}		✓	
Recombination time τ_r	✓		✓

account for slopes where $s < -4$. As a consequence, to adjust experimental and modeling results of Fig. 4, we have considered that the recombination time τ_r evolves as:

$$\tau_r(F_{1\omega}, F_{3\omega}) = \frac{t_1}{1 + \exp\left(\frac{F_{1\omega} - F_{1\omega}^{(0)}}{C_1 \times F_{3\omega}}\right)} + t_2 \quad (7)$$

where t_1 and t_2 refer to time durations and are constant, C_1 is also a constant and $F_{1\omega}^{(0)}$ corresponds to the $F_{1\omega}$ fluence threshold between a multi-photon and an avalanche regime. In the model, $t_1 = 1,400$ ps, $t_2 = 100$ ps, $F_{1\omega}^{(0)} = 27$ J/cm² and $C_1 = 0.3$.

Figure 6 represents the evolution of τ_r as a function of the fluences $F_{1\omega}$ and $F_{3\omega}$ obtained with the expression defined in Eq. (7) where it appears that the distribution evolves from a step-like function to a slowly decreasing function.

The previous dependence of τ_r on $F_{1\omega}$ and $F_{3\omega}$ is supported by the study of Duchateau et al. [37] showing that relaxation dynamics depend on the photon energy and the laser intensity in KDP crystal. More precisely, due to the formation of new defects (traps), the relaxation time decreases when intensity increases [37]. The proposed variations of τ_r given by Eq. (7) and Fig. 6 are consistent with the previously observed behavior.

To support this analysis, we have carried out a complementary experiment allowing us to evaluate τ_r . This experiment consists in introducing a variable time delay between the pulses at 1ω and 3ω . Delays are obtained by adjusting 1ω or 3ω optical pathways in order to obtain negative delays (the 1ω radiation first interacts with the crystal) or positive ones. The couple of fluences $(F_{1\omega}, F_{3\omega}) = (15, 10)$ J/cm² have been chosen to make the 3ω radiation the dominant mechanism (i.e., fluences at 1ω , if taken separately, are not sufficient to induce breakdown by themselves). It is noteworthy that slight discrepancies have been observed between the predetermined and experimentally obtained fluences.

Figure 7 exhibits the evolution of the damage probability P_{dam} as a function of the time delay between the 1ω and 3ω beams. In region 1 (i.e., $\Delta\tau < 0$), $P_{\text{dam}}(F_{1\omega}, F_{3\omega})$ is constant on average (around 50 %, called $P_{(50\%)}$). We have checked that the variations are due to the above-mentioned fluence fluctuations. This indicates there is no coupling effect in region 1. In region 2, a coupling effect is observed between these two wavelengths since P_{dam} increases. This coupling becomes more and more efficient as long as the optical delay $\Delta\tau$ is shorter than 4.5 ns. In region 3, when $\Delta\tau > 4.5$ ns, the probability begins to vanish, thus suggesting a decrease in the coupling. Indeed, P_{dam} goes back down to $P_{(50\%)}$ at a delay close to the pulse duration. This suggests that the plasma recombines on a timescale much shorter than the pulse duration. Given the

Fig. 6 Evolution of the recombination time τ_r as a function of the fluences $F_{1\omega}$ and $F_{3\omega}$, where τ_r is defined by Eq. (7)

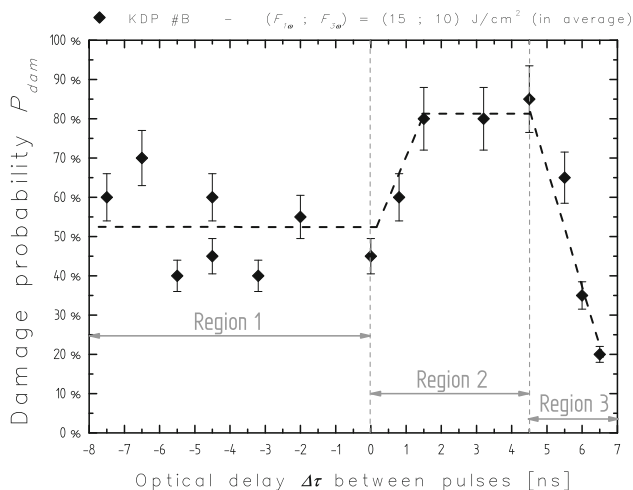
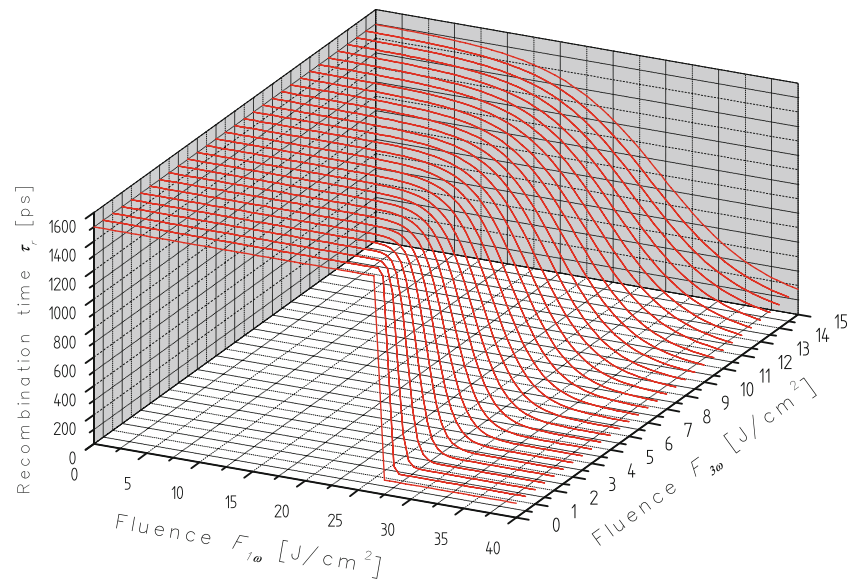


Fig. 7 Evolution of P_{dam} as a function of the optical delay between the 1ω and 3ω pulses, for different couples of fluences $F_{1\omega}$ and $F_{3\omega}$. Dashed lines are guide for the eyes

delay resolution of this experiment, we conclude that τ_r is in the order of 1 ns or less, which is consistent with the modeling results. Note that DeMange et al. have suggested in [17] a value close to 500 ps.

5 Conclusion

In this study, we have compared in the ns regime several experimental and modeling results with various fluence ratios and wavelengths. First, we have developed a model which accounts for avalanche as a mechanism possibly responsible for optical breakdown at 1ω . Then, in wavelength mixing configuration, the experimental observations

indicate the existence of a coupling effect between ionization mechanisms which are strongly sensitive to wavelength. These observations have been supported by the modeling work which shows that not only a multi-photon process, but also an avalanche can be responsible for permanent modifications of the material. Also, some striking features have been observed. In the competition regime where fluences at 1ω are much greater than at 3ω , it has been shown that II can dominate and prevail over MPI. The coupling regime is observed when fluence ratios at 3ω and 1ω do not exceed 1:3. Furthermore, we have highlighted that the recombination time has a strong influence on the breakdown mechanism. Our conclusions indicate that it depends on the radiation intensity suggesting that the formation of new defects is involved during the damage event. The value of the recombination time is estimated to be 1 ns or less.

Appendix 1: DMT model: general presentation

The DMT approach has been developed at 3ω by Dyan et al. [21]. KDP is supposed to contain nanometer-scale defects that may initiate laser damage when temperature exceeds a given critical temperature. The model solves the 3D heat equation of these nanometer plasma balls whose absorption efficiency is described through the Mie theory [38], introducing both wavelength and size dependence. The plasma optical indices mandatory to Mie theory equations are then evaluated within the Drude model [30]. The resolution of the Fourier's equation [39, 40] gives the defect temperature evolution as a function of its radius a . Thus in the mono-wavelength case, the temperature elevation $\theta_{(\omega)}$ of the defect reads:

$$\theta_{(\omega)} = Q_{\text{abs}}^{(\omega)} I_{(\omega)} \frac{\xi \sqrt{4\kappa_{\text{KDP}} \tau_L}}{4\lambda_{\text{KDP}}} \quad (8)$$

where $Q_{\text{abs}}^{(\omega)}$, $I_{(\omega)}$ and τ_L are the absorption efficiency, the laser intensity and the pulse duration for the ω frequency. κ_{KDP} and λ_{KDP} are the diffusivity and the thermal conductivity of the KDP. ξ is a function taking into account the material properties [21]. The critical fluence F_c necessary to reach the critical temperature T_c for which a first damage site occurs can be written as [21]:

$$F_c = \gamma \frac{T_c - T_0}{Q_{\text{abs}}(a_c)} \sqrt{\tau_L} \quad (9)$$

where γ is a factor depending on the material properties, T_0 is the room temperature and a_c is the defect critical radius which is associated with T_c , usually close to 100 nm. Assuming that a damage site appears as soon as the critical temperature T_c is reached, and then considering that any fluence $F_{(\omega)}$ activates the precursor defects in a defined size range [17, 20, 21, 26, 41], the damage density ρ_{dam} as a function of the fluence $F_{(\omega)}$ can be finally extracted from the following expression:

$$\rho_{\text{dam}}(F) = \int_{a_-(F)}^{a_+(F)} D_{\text{def}}(a) \cdot da \quad (10)$$

where $[a_-(F), a_+(F)]$ is the range of defects size for which $T = T_c$, $D_{\text{def}}(a)$ is the density size distribution of absorbers assumed to be:

$$D_{\text{def}}(a) = \frac{C}{a^{p+1}} \quad (11)$$

where C and p are adjusting parameters. This distribution is consistent with the fact that the more numerous the precursors, the higher is the damage probability. By integrating Eq. (10), we thus obtain:

$$\rho_{\text{dam}}(F) = \frac{C}{p} \left(\frac{1}{a_-^p(F)} - \frac{1}{a_+^p(F)} \right). \quad (12)$$

As $\frac{1}{a_+^p(F)}$ is smaller than $\frac{1}{a_-^p(F)}$, only absorbers whose size is smaller than the critical size a_c contribute significantly to $\rho_{\text{dam}}(F)$. Also, it can be shown that in the neighborhood of F_c and for $a < a_c$, the damage fluence can be written as $F \propto \frac{1}{a}$. It results that the damage density ρ_{dam} evolves as a function of the laser fluence F as:

$$\rho_{\text{dam}}(F) \simeq \frac{C}{p} \frac{1}{a_-^p(F)} \propto \frac{C}{p} F^p. \quad (13)$$

Thus, ρ_{dam} evolves as a power law function of the fluence, where C and p can be determined to fit the experimental data.

Appendix 2: Derivation of t_{heat}

Mono-wavelength case

The evolution of the electronic density in the conduction band is given by the following rate equation:

$$\frac{\partial n_{\text{cb}}}{\partial t} = \sigma_m \Phi_{\text{ph}}^m n_{\text{vb}} - \frac{n_{\text{cb}}}{\tau_r} \quad (14)$$

where σ_m is the m -photon absorption cross section, Φ_{ph} is the photon flux at 1ω ($= \frac{F}{\hbar\omega\tau_L}$) and τ_r is the recombination time. Note that σ_m may account for assisted transitions with states located in the bandgap as suggested by Carr et al. [6] in their previous studies.

By integrating Eq. (14), assuming that for $t = 0$ $n_{\text{cb}} = 0$, the electronic density n_{cb} reads as:

$$n_{\text{cb}}(t) = n_{\text{vb}} \times (\sigma_m \Phi_{\text{ph}}^m) \tau_r \left[1 - e^{-\frac{t}{\tau_r}} \right]. \quad (15)$$

Then, for $t = t_{\text{aval}}$, which is the criterion for the avalanche to trigger, associated with the minimum density n_{aval} (one electron in the defect volume), Eq. (15) becomes:

$$t_{\text{prod}} = -\tau_r \times \ln \left(1 - \frac{n_{\text{aval}} (\hbar\omega\tau_L)^m}{n_{\text{vb}} \sigma_m F^m \tau_r} \right). \quad (16)$$

Also, the heating time t_{heat} is defined by the following relation:

$$t_{\text{heat}} = \tau_L - t_{\text{prod}}. \quad (17)$$

To simplify, we assume $K_1 = n_{\text{vb}} \frac{\sigma_m F^m}{(\hbar\omega\tau_L)^m}$, which results in:

$$t_{\text{heat}} = \tau_L + \tau_r \times \ln \left(1 - \frac{n_{\text{aval}}}{K_1 \tau_r} \right). \quad (18)$$

Thus, according to Eq. (18), there exists a heating time such as $0 < t_{\text{heat}} < 6.5$ ns if the condition $\ln \left(1 - \frac{n_{\text{aval}}}{K_1 \tau_r} \right) < 0$ is verified. At the same time, it is possible to define the fluence, referred to as F_{aval} for which $t_{\text{heat}} > 0$. F_{aval} is then defined by Eq. (19):

$$F_{\text{aval}} > \frac{1}{\left[\left(1 - e^{-\frac{\tau_L}{\tau_r}} \right) \frac{n_{\text{cb}}}{n_{\text{aval}}} \tau_r \right]^{\frac{1}{m}}} \times \frac{1}{\hbar\omega\tau_L}. \quad (19)$$

Multi-wavelength case

Since 1ω and 3ω are assumed to both produce the electronic density in the conduction band, it results in the following rate equation:

$$\frac{\partial n_{\text{cb}}}{\partial t} = (\sigma_m \Phi_{\text{ph}}^m + \sigma_3 \Phi_{\text{ph}}^3) n_{\text{vb}} - \frac{n_{\text{cb}}}{\tau_r}. \quad (20)$$

The determination of t_{heat} has been previously proposed in Appendix 2.1. When now considering two radiations at

the same time, with a mean pulse duration $\overline{\tau_L}$ corresponding to $\overline{\tau_L} = \frac{\tau_L^{1\omega} + \tau_L^{3\omega}}{2}$, the mathematical derivation remains the same and t_{heat} becomes:

$$t_{\text{heat}} = \overline{\tau_L} + \tau_r \times \ln\left(1 - \frac{n_{\text{aval}}}{K'_1 \tau_r}\right) \quad (21)$$

where K'_1 is defined by:

$$K'_1 = n_{vb} \left(\frac{\sigma_m F_{1\omega}^m}{(\hbar \omega_1 \tau_L^{1\omega})^m} + \frac{\sigma_3 F_{3\omega}^3}{(\hbar \omega_3 \tau_L^{3\omega})^3} \right). \quad (22)$$

References

1. N. Bloembergen, Laser-induced electric breakdown in solids. *IEEE J. Quantum Electron.* **10**, 375–386 (1974)
2. S. Jones, P. Brunlich, R. Casper, X.-A. Shen, P. Kelly, Recent progress on laser-induced modifications and intrinsic bulk damage of wide-gap optical materials. *Opt. Eng.* **28**, 1039 (1989)
3. D. Arnold, E. Cartier, Theory of laser-induced free-electron heating and impact ionization in wide-band-gap solids. *Phys. Rev. B* **46**(23), 15102–15115 (1992)
4. P.K. Kennedy, A first-order model for computation of laser-induced breakdown thresholds in ocular and aqueous media—part I: theory. *IEEE Quantum Electron.* **31**, 2241–2249 (1995)
5. D.W. Fradin, E. Yablonovitch, M. Bass, Confirmation of an electron avalanche causing laser-induced bulk damage at 1.06 μm . *Appl. Opt.* **12**(4), 700 (1973)
6. C.W. Carr, H.B. Radousky, S.G. Demos (2003) Wavelength dependence of laser-induced damage: determining the damage initiation mechanisms. *Phys. Rev. Lett.* **91**(12), 127402 (2003)
7. L.V. Keldysh, Ionization in the field of a strong electromagnetic wave. *Sov. Phys. JETP* **20**, 1307 (1965)
8. B. Gorshkov, A. Epifanov, A. Manenkov, Avalanche ionization produced in solids by large radiation quanta and relative role of multiphoton ionization in laser-induced breakdown. *Sov. Phys. JETP* **49**, 309–315 (1979)
9. F. Docchio, P. Regondi, M.R.C. Capon, J. Melleri, Study of the temporal and spatial dynamics of plasmas induced in liquids by nanosecond Nd:Yag laser pulses: 1 analysis of the plasma starting times. *Appl. Opt.* **27**(17), 3361–3668 (1988)
10. A. Kaiser, B. Rethfeld, M. Vicanek, G. Simon, Microscopic processes in dielectrics under irradiation by subpicosecond laser pulses. *Phys. Rev. B* **61**, 11437 (2000)
11. B. Rethfeld, Unified model for the free-electron avalanche in laser-irradiated dielectrics. *Phys. Rev. Lett.* **92**(18), 187401 (2004)
12. M. Sparks, D.L. Mills, R. Warren, T. Holstein, A.A. Maradudin, L.J. Sham, E. Loh Jr., D.F. King, Theory of electron-avalanche breakdown in solids. *Phys. Rev. B* **24**(6), 3519–3536 (1981)
13. X.A. Shen, S.C. Jones, P. Brunlich, Laser heating of free electrons in wide-band-gap optical materials at 1064 nm. *Phys. Rev. Lett.* **62**(23), 2711–2713
14. A. Vaidyanathan, T.W. Walker, A.H. Guenther, The relative roles of avalanche multiplication and multiphoton absorption in laser-induced damage of dielectrics. *IEEE J. Quantum Electron.* **16**, 1 (1980)
15. A.A. Manenkov, New results on avalanche ionization as a laser damage mechanism in transparent dielectrics. *Natl. Bureau Stand. Spec. Publ.* **509**, 455–464 (1986)
16. B.C. Stuart, M.D. Feit, A.M. Rubenchik, B.W. Shore, M.D. Perry, Laser-induced damage in dielectrics with nanosecond to subpicosecond pulses. *Phys. Rev. Lett.* **74**, 2248 (1995)
17. P. DeMange, R.A. Negres, A.M. Rubenchik, H.B. Radousky, M.D. Feit, S.G. Demos, The energy coupling efficiency of multiwavelength laser pulses to damage initiating defects in deuterated KH_2PO_4 nonlinear crystals. *J. Appl. Phys.* **103**, 083122 (2008)
18. S. Reyné, G. Duchateau, J.-Y. Natoli, L. Lamaignère, Pump–pump experiment in KH_2PO_4 crystals: coupling two different wavelengths to identify the laser-induced damage mechanisms in the nanosecond regime. *Appl. Phys. Lett.* **96**, 121102–121104 (2010)
19. L. Lamaignère, M. Balas, R. Courchinoux, T. Donval, J.C. Poncetta, S. Reyné, B. Bertussi, H. Bercegol, Parametric study of laser-induced surface damage density measurements: toward reproducibility. *J. Appl. Phys.* **107**, 023105 (2010)
20. M.D. Feit, A.M. Rubenchik, Implications of nanoabsorber initiators for damage probability curves and pulselength scaling and laser conditioning. In: *Proc. SPIE* 5273, pp. 527374–527382
21. A. Dyan, F. Enguehard, S. Lallich, H. Piombini, G. Duchateau, Scaling laws in laser-induced KDP crystal damage by nanosecond pulses at 3ω . *J. Opt. Soc. Am. B* **25**(6), 1087–1095 (2008)
22. M.D. Feit, A.M. Rubenchik, J.B. Trenholme, Simple model of laser damage initiation and conditioning in frequency conversion crystals. In: *Proc. SPIE* 5991, p. 59910W
23. G. Duchateau, A. Dyan, Coupling statistics and heat transfer to study laser-induced crystal damage by nanosecond pulses. *Opt. Express* **15**(8), 4557–4576 (2007)
24. G. Duchateau, Simple models for laser-induced damage and conditioning of potassium dihydrogen phosphate crystals by nanosecond pulses. *Opt. Express* **17**(13), 10434–10456 (2009)
25. S.G. Demos, P. DeMange, R.A. Negres, M.D. Feit, Investigation of the electronic and physical properties of defect structures responsible for laser-induced damage in DKDP crystal. *Opt. Express* **18**(12), 13788–13804 (2010)
26. S. Reyné, G. Duchateau, J.-Y. Natoli, L. Lamaignère, Laser-induced damage of KDP crystals by 1ω nanosecond pulses: influence of crystal orientation. *Opt. Express* **17**(24), 21652–21665 (2009)
27. ISO Standard No 21254-1 (2011); ISO Standard No 21254-2 (2011); ISO Standard No 21254-3 (2011)
28. L. Lamaignère, T. Donval, M. Loiseau, J.C. Poncetta, G. Razé, C. Meslin, B. Bertussi, H. Bercegol, Accurate measurements of laser-induced bulk damage density. *Meas. Sci. Technol.* **20**, 095701 (2009)
29. S. Juodkazis, K. Nishimura, S. Tanaka, H. Misawa, E. Gamaly, B. Luther-Davies, L. Hallo, P. Nicolai, V. Tikhonchuk, Laser induced microexplosion confined in the bulk of a sapphire crystal: evidence of multimegabar pressures. *Phys. Rev. Lett.* **96**, 166101 (2006)
30. R.E. Hummel, *Electronic properties of materials*, 3rd edn. (Springer, New York)
31. J. Noack, A. Vogel, Laser-induced plasma formation in water at nanosecond to femtosecond time scales: calculation of thresholds, absorption coefficients, and energy density. *IEEE J. Quantum Electron.* **35**, 1156–1167 (1999)
32. P. Agostini, G. Petite, Photoelectric effect under strong irradiation. *Contemp. Phys.* **29**, 55–77 (1988)
33. P. DeMange, C.W. Carr, R.A. Negres, H.B. Radousky, S.G. Demos, Multiwavelength investigation of laser-damage performance in potassium dihydrogen phosphate after laser annealing. *Opt. Lett.* **30**(3), 221–223 (2005)
34. P. DeMange, R.A. Negres, A.M. Rubenchik, Understanding and predicting the damage performance of $\text{K}_2\text{H}_{(2-x)}\text{D}_x\text{PO}_4$ crystal under simultaneous exposure to 532- and 355-nm pulses. *Appl. Phys. Lett.* **89**, 181922 (2006)
35. P. DeMange, R.A. Negres, C.W. Carr, H.B. Radousky, S.G. Demos, Laser-induced defect reactions governing damage initiation in DKDP crystals. *Opt. Express* **14**(12), 5313–5328 (2006)

36. P. DeMange, R.A. Negres, H.B. Radousky, S.G. Demos, Differentiation of defect populations responsible for bulk laser-induced damage in potassium dihydrogen phosphate crystals. *Opt. Eng.* **45**(10), 104205 (2006)
37. G. Duchateau, G. Geoffroy, A. Dyan, H. Piombini, S. Guizard, Electron-hole dynamics in normal and deuterated KH_2PO_4 illuminated by intense femtosecond laser pulses. *Phys. Rev. B* **83**(7), 075114 (2011)
38. H.C. Van de Hulst, *Light scattering by small particles* (Dover publications Inc., New York, 1981)
39. R.W. Hopper, D.R. Uhlmann, Mechanism of inclusion damage in laser glass. *J. Appl. Phys.* **41**(10), 4023–4037 (1970)
40. H.S. Carslaw, J.C. Jaeger, *Conduction of heat in solids*, 2nd edn. (Oxford Science Publications, Oxford)
41. S. Reyn , M. Loiseau, G. Duchateau, J.-Y. Natoli, L. Lamaign re, Towards a better understanding of multi-wavelength effects on KDP crystals. In: *Proc. SPIE 7361*, p. 73610Z (2009)